Coulomb breakup of ^{11}Be and ^{19}C

P. Banerjee, I. J. Thompson, and J. A. Tostevin
Department of Physics, School of Physical Sciences, University of Surrey, Guildford, Surrey GU2 5XH, United Kingdom
(Received 18 March 1998)

We investigate the Coulomb part of the one-neutron removal cross section in breakup reactions of the neutron rich nuclei ^{11}Be and ^{19}C. Approximate Coulomb breakup amplitudes are derived from two distinct theoretical viewpoints. One of these uses an approximation to the distorted-wave Born approximation. The other assumes an adiabatic treatment of the projectile excitation to the low energy continuum. Both approaches include approximately the finite range of the interaction between the breakup fragments and so can treat non-s-wave projectiles. Calculations are analyzed and compared with available experimental data for total one-neutron removal cross sections, neutron angular distributions, heavy charged fragment momentum distributions, and excitation energy spectra for breakup on high Z targets. [S0556-2813(98)00108-3]

PACS number(s): 24.10.Eq, 25.60.−t, 25.70.Mn

I. INTRODUCTION

Experiments with beams of neutron rich nuclei, like ^{11}Li, ^{11}Be, and ^{14}Be, have revealed the existence of a neutron halo structure. In their ground states these nuclei have valence neutron(s) which extend far out in space beyond a smaller dense core [1–3]. ^{19}C, the last particle stable odd-neutron isotope of carbon, also promises to be a halo candidate [4,5] with a very small one-neutron separation energy of 242 $\pm$95 keV [6]. Such systems provide a stringent test of nuclear structure models developed for stable nuclei as they involve new structures and surface phenomena. The halo structure is manifest experimentally through large reaction and Coulomb dissociation cross sections [7–9], forward peaked angular distributions of neutrons measured in coincidence with the core nuclei [10,11], a narrow component in the neutron angular distributions in core breakup reactions [5], and extremely narrow measured momentum distributions of these core nuclei [12–14].

Consideration of the fragmentation of these halo nuclei is important. Most have only one bound state, the ground state, and a broad featureless continuum. Thus conventional nuclear structure methods, dealing with the energies and spin-parities of excited levels, are inappropriate. One must consider processes that excite the continuum and the study of breakup reactions provides such a tool. In particular, a precise knowledge of halo nucleus Coulomb dissociation cross sections would place constraints on their electric dipole response [15–19].

The Coulomb dissociation of ^{11}Li and ^{11}Be has been studied by Canto *et al.* [20] and Bertulani *et al.* [21] within a semiclassical coupled-channels formalism. Kido *et al.* [22] and Bertsch *et al.* [23,24] have solved the time-dependent Schrödinger equation for the relative motion of the core and halo. The results in [22–24] are however dependent on the range of impact parameters chosen for the assumed straight line trajectories used to describe the motion of the projectile in the field of the target. Shyam *et al.* [25,26] have studied the Coulomb breakup of several neutron dripline nuclei using the post form of the distorted-wave Born approximation (DWBA) theory. However, they make the simplifying approximation of a zero-range (ZR) interaction between the constituents of the projectile, as did the authors of [20,21]. Other semiclassical [11] and prior form DWBA [16] calculations also make the ZR approximation.

A consequence of using the ZR approximation is that the structure of the projectile is assumed to affect the breakup amplitude only as a multiplicative constant. Although the ZR approximation is justified in studies of low energy deuteron breakup [27–29], its use for more massive projectiles at higher beam energies is very suspect. The approximation is certainly inapplicable in cases where the projectile's internal orbital angular momentum is different from zero, when it is crucial to include the effects of the finite-range of the interaction. This in turn introduces a more complex dependence and sensitivity of the breakup amplitude to the projectile structure.

In this paper we report approximate finite-range quantum mechanical calculations of elastic Coulomb breakup in ^{11}Be and ^{19}C induced reactions at beam energies below 100 MeV/nucleon. We derive finite-range breakup amplitudes from two theoretically distinct viewpoints. One of these makes an approximation to the distorted waves Born approximation theory. The other assumes an adiabatic treatment of the projectile excitation to the low energy continuum. Calculations of the exclusive neutron angular distributions, parallel and transverse momentum distributions of the core fragment, and excitation energy spectra are also presented. In Sec. II we present details of the theoretical formulations. Structure models used for ^{11}Be and ^{19}C are presented in Sec. III. Our results are discussed in Sec. IV and conclusions are drawn in Sec. V.

II. THREE-BODY MODEL OF COULOMB BREAKUP

We consider the elastic Coulomb breakup of a two-body composite projectile $a=c+v$, with spins s_a, s_c, and s_v, from a spinless target t. Thus we treat the $a+t\rightarrow c+v+t$ dissociation process as an effective three-body problem, which are assumed to have masses m_c, m_v, and m_t. We also assume that the valence particle v is uncharged and does not interact with the target, $V_{vt}=0$, and that the charged core c interacts with the target through a (spin-independent) point

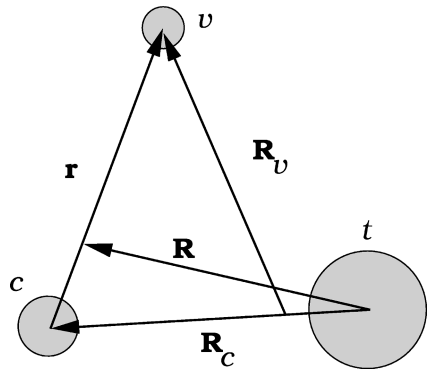

FIG. 1. The coordinate system adopted for the core, valence particle, and target three-body system.

Coulomb interaction V_{ct}. We adopt the Jacobi system of coordinates shown in Fig. 1.

The Schrödinger equation satisfied by the three-body scattering wave function, for the projectile incident with momentum $\hbar\boldsymbol{k}_a$ and spin-projection σ_a in the center-of-mass (c.m.) frame, is therefore

$$[T_{\boldsymbol{R}}+V_{ct}(\boldsymbol{R}-\gamma\boldsymbol{r})+H_{cv}-E]\Psi^{(+)}_{\boldsymbol{k}_a\sigma_a}(\boldsymbol{r},\boldsymbol{R})=0, \tag{1}$$

where $\gamma=m_v/(m_c+m_v)$ and H_{cv} is the internal Hamiltonian for the valence-core system. $T_{\boldsymbol{R}}$ is the kinetic energy operator for the projectile-target relative motion. The projectile ground state will be denoted $\Phi_{a\sigma_a}(\boldsymbol{r})$, with an assumed separation energy $-\epsilon_0$, and is obtained by solving the Schrödinger equation for the core-valence particle relative motion in their binding potential $V_{cv}(\boldsymbol{r})$.

The transition amplitude for elastic Coulomb breakup, in the c.m. frame, is

$$T_{\sigma_c\sigma_v;\sigma_a}=\langle\chi^{(-)}(\boldsymbol{k}_c,\boldsymbol{R}_c)\mathcal{S}_{\sigma_c}e^{i\boldsymbol{k}_v\cdot\boldsymbol{R}_v}\mathcal{S}_{\sigma_v}|V_{cv}|\Psi^{(+)}_{\boldsymbol{k}_a\sigma_a}(\boldsymbol{r},\boldsymbol{R})\rangle, \tag{2}$$

where $\mathcal{S}_{\sigma_c}$ and $\mathcal{S}_{\sigma_v}$ are the core and valence particle internal wave functions with σ_c and σ_v their spin projections. $\hbar\boldsymbol{k}_c$ and $\hbar\boldsymbol{k}_v$ are the asymptotic momenta of these fragments, conjugate to $\boldsymbol{R}_c$ and $\boldsymbol{R}_v$, respectively, and $\chi^{(-)}$ is an in-going waves Coulomb distorted wave function describing the c–t relative motion in the final state. Since it is assumed that $V_{vt}=0$ the valence particle is described by a plane wave in the final state.

A. DWBA and adiabatic approximation schemes

We outline two approximation schemes for calculations of the exact quantum mechanical amplitude Eq. (2) based on (i) an approximation to the distorted-wave Born approximation (DWBA), and (ii) an adiabatic treatment of the projectile's excitation [30,31]. We show that, dependent on the precise assumptions made in the first of these methods, the formulas derived from the two approaches can look similar, or even identical. We stress however that in deriving these formulas the two models make quite distinct physical approximations to the exact three-body wave function $\Psi^{(+)}$. Possible observable differences between calculations based on the two approaches are discussed with our results. The basis of the two formulations is first clarified.

In the DWBA it is assumed that Coulomb excitations of the projectile are weak and so need be treated only to first order. $\Psi^{(+)}$ is therefore approximated, as is usual, by the product

$$\Psi^{(+)}_{\boldsymbol{k}_a\sigma_a}(\boldsymbol{r},\boldsymbol{R})\approx\Psi^{\mathrm{DW}}_{\boldsymbol{k}_a\sigma_a}(\boldsymbol{r},\boldsymbol{R})=\Phi_{a\sigma_a}(\boldsymbol{r})\chi^{(+)}(\boldsymbol{k}_a,\boldsymbol{R}). \tag{3}$$

Here $\chi^{(+)}$ is a Coulomb distorted wave describing the (point) projectile elastic scattering and, by definition, Ψ^{DW} has a vanishing overlap with all projectile inelastic channels. Substituted in Eq. (2) this yields the usual post form transition amplitude T^{DW} of DWBA theory.

By contrast, the adiabatic approach does not assume the breakup states are weakly coupled. It is assumed however that the states which are strongly coupled to the projectile ground state in Eq. (1) have c–v relative energies $E_{cv}\ll E$, or that the energies associated with H_{cv} are small. H_{cv} is therefore replaced by a representative (constant) energy, taken as $-\epsilon_0$. It was shown in Ref. [30] that the resulting (adiabatic) three-body equation has an exact solution which separates in the variables $\boldsymbol{R}_c$ and $\boldsymbol{r}$, namely

$$\Psi^{(+)}_{\boldsymbol{k}_a\sigma_a}(\boldsymbol{r},\boldsymbol{R})\approx\Psi^{\mathrm{AD}}_{\boldsymbol{k}_a\sigma_a}(\boldsymbol{r},\boldsymbol{R})=\Phi_{a\sigma_a}(\boldsymbol{r})e^{i\gamma\boldsymbol{k}_a\cdot\boldsymbol{r}}\chi^{(+)}(\boldsymbol{k}_a,\boldsymbol{R}_c). \tag{4}$$

The $\chi^{(+)}$ here is the same Coulomb distorted wave as appeared in Eq. (3) but is evaluated at the core coordinate $\boldsymbol{R}_c$. Unlike Ψ^{DW}, Ψ^{AD} solves the adiabatic three-body equation and by construction it retains breakup components—evident from its complicated dependence on $\boldsymbol{r}$. This approximate three-body solution, when substituted in Eq. (2), derives the adiabatic approximation to the elastic breakup amplitude T^{AD} [31].

In both cases the projectile ground state appears as a factor, which we now write explicitly, to clarify its orbital components l, as

$$\Phi_{a\sigma_a}(\boldsymbol{r})=\sum_{l\mu jm\sigma_c'\sigma_v'}\langle s_c\sigma_c' jm|s_a\sigma_a\rangle \times\langle l\mu s_v\sigma_v'|jm\rangle\Phi_a^{l\mu}(\boldsymbol{r})\mathcal{S}_{\sigma_c'}\mathcal{S}_{\sigma_v'}, \tag{5}$$

where $\Phi_a^{l\mu}(\boldsymbol{r})=i^l u_l(r)Y_{l\mu}(\hat{\boldsymbol{r}})$, the u_l are radial wave functions, and the $Y_{l\mu}$ are the spherical harmonics. Since the only distorting interaction V_{ct} is assumed central the integrations over spin variables can be carried out in Eq. (2). The required (AD and DW) approximate transition amplitudes can then be expressed as

$$T_{\sigma_c\sigma_v;\sigma_a}=\sum_{l\mu jm}\langle s_c\sigma_c jm|s_a\sigma_a\rangle\langle l\mu s_v\sigma_v|jm\rangle\beta_{l\mu}, \tag{6}$$

where the reduced transition amplitudes $\beta_{l\mu}$ are, in the DWBA

$$\beta^{\mathrm{DW}}_{l\mu}=\langle\chi^{(-)}(\boldsymbol{k}_c,\boldsymbol{R}_c)e^{i\boldsymbol{k}_v\cdot\boldsymbol{R}_v}|V_{cv}|\Phi_a^{l\mu}(\boldsymbol{r})\chi^{(+)}(\boldsymbol{k}_a,\boldsymbol{R})\rangle, \tag{7}$$

and in the adiabatic model

$$\beta_{l\mu}^{\mathrm{AD}}=\langle\chi^{(-)}(\boldsymbol{k}_c,\boldsymbol{R}_c)e^{i\boldsymbol{k}_v\cdot\boldsymbol{R}_v}|V_{cv}|\Phi_a^{l\mu}(\boldsymbol{r})e^{i\gamma\boldsymbol{k}_a\cdot\boldsymbol{r}}\chi^{(+)}(\boldsymbol{k}_a,\boldsymbol{R}_c)\rangle. \tag{8}$$

Since $\boldsymbol{R}_v=\alpha\boldsymbol{R}_c+\boldsymbol{r}$, where $\alpha=m_t/(m_t+m_c)$, then without further approximation the entire adiabatic amplitude now separates exactly in the coordinates $\boldsymbol{R}_c$ and $\boldsymbol{r}$, as

$$\begin{aligned}\beta_{l\mu}^{\mathrm{AD}}&=\langle e^{i\vec{q}_v\cdot\boldsymbol{r}}|V_{cv}|\Phi_a^{l\mu}(\boldsymbol{r})\rangle\\&\quad\times\langle\chi^{(-)}(\boldsymbol{k}_c,\boldsymbol{R}_c)e^{i\alpha\boldsymbol{k}_v\cdot\boldsymbol{R}_c}|\chi^{(+)}(\boldsymbol{k}_a,\boldsymbol{R}_c)\rangle\\&=\langle\vec{q}_v|V_{cv}|\Phi_a^{l\mu}\rangle\langle\chi^{(-)}(\boldsymbol{k}_c);\alpha\boldsymbol{k}_v|\chi^{(+)}(\boldsymbol{k}_a)\rangle.\end{aligned} \tag{9}$$

The momentum $\boldsymbol{q}_v$ appearing in the first term is $\boldsymbol{q}_v=\boldsymbol{k}_v-\gamma\boldsymbol{k}_a$.

B. Effective momentum approximation to DWBA

The entrance channel distorted wave function in β^{DW} does not separate in the variables $\boldsymbol{R}_c$ and $\boldsymbol{r}$. The DWBA amplitude thus remains a six dimensional integral. An approximate variable separation, and hence factorization of the amplitude, can however be developed if one assumes, e.g., [32,33], a local momentum approximation to the entrance channel Coulomb distorted wave for $\boldsymbol{R}(=\boldsymbol{R}_c+\gamma\boldsymbol{r})$ values about the point $\boldsymbol{R}_c$, i.e.,

$$\chi^{(+)}(\boldsymbol{k}_a,\boldsymbol{R})\approx\exp(i\gamma\boldsymbol{K}_a\cdot\boldsymbol{r})\chi^{(+)}(\boldsymbol{k}_a,\boldsymbol{R}_c). \tag{10}$$

Equation (10) is of course an exact Taylor series expansion about $\boldsymbol{R}_c$ if $\boldsymbol{K}_a(=-i\nabla_{\boldsymbol{R}_c})$ is treated exactly. This is not done here. Rather $\boldsymbol{K}_a\equiv\boldsymbol{K}_a(R_D)$ will be interpreted as an *effective momentum* for the projectile, to be evaluated at a representative distance R_D from the target, where the integrand in Eq. (7) is thought to be large. The choice of direction of this vector is discussed later, however, since V_{cv} restricts the integrals in Eq. (7) to small $|\boldsymbol{r}|$, Eq. (10) may be a useful first approximation.

It was shown in [32] that a condition for the validity of a local momentum approximation is that the variation of the magnitude $K_a=|\boldsymbol{K}_a|$ with position R_D should satisfy

$$\mathcal{R}_{cv}\ll\frac{K_a(R_D)}{2}\left|\frac{dK_a(r)}{dr}\right|^{-1}_{r=R_D}, \tag{11}$$

where $\mathcal{R}_{cv}$ is of order of the range of V_{cv}. We will show that for the reactions of interest this condition on K_a is satisfied. In the following Eq. (10) will be used assuming a *fixed* value of $\boldsymbol{K}_a$ for all $\boldsymbol{R}$, but whose direction, when used in Eq. (7), can be allowed to depend on $\boldsymbol{k}_c$ and $\boldsymbol{k}_v$. Equation (10) provides a separation of the six dimensional integral in β^{DW} which then reads

$$\beta_{l\mu}^{\mathrm{DW}}=\langle\vec{Q}_v|V_{cv}|\Phi_a^{l\mu}\rangle\langle\chi^{(-)}(\boldsymbol{k}_c);\alpha\boldsymbol{k}_v|\chi^{(+)}(\boldsymbol{k}_a)\rangle. \tag{12}$$

Now, in the first term, $\vec{Q}_v=\boldsymbol{k}_v-\gamma\boldsymbol{K}_a$, where $\boldsymbol{K}_a$ is the effective momentum which has yet to be specified.

The two factors in Eqs. (9) and (12) also separate the structure and dynamical parts of the calculations. The first terms carry all information about the structure of the projectile—through its ground state wave function. These are the same vertex functions as arise in transfer reaction calculations and can be written

$$\langle\boldsymbol{q}|V_{cv}|\Phi_a^{l\mu}\rangle=D_l(q)Y_{l\mu}(\hat{\boldsymbol{q}})=D(\boldsymbol{q}), \tag{13}$$

where

$$D_l(q)=4\pi\int_0^\infty drr^2j_l(qr)V_{cv}(r)u_l(r). \tag{14}$$

The second factors, the overlaps $\langle\chi^{(-)}(\boldsymbol{k}_c);\alpha\boldsymbol{k}_v|\chi^{(+)}(\boldsymbol{k}_a)\rangle$, are identical in Eqs. (9) and (12). These can also be evaluated in closed form using the bremsstrahlung integral [34] and are associated solely with the reaction dynamics.

C. Comparison of model amplitudes

From the computational point of view, the reaction amplitudes β^{DW} and β^{AD} differ only through the momenta which appear in the first terms, the vertex functions. The amplitudes become identical in the limit that we choose $\boldsymbol{K}_a=K_a(R_D=\infty)\hat{\boldsymbol{k}}_a\equiv\boldsymbol{k}_a$. The factors $\langle\chi^{(-)}(\boldsymbol{k}_c);\alpha\boldsymbol{k}_v|\chi^{(+)}(\boldsymbol{k}_a)\rangle$, and hence the treatment of the reaction dynamics, are treated identically in the two cases.

While Eqs. (9) and (12) appear very similar, we stress that they result from quite distinct approximations to the three-body wave function $\Psi^{(+)}$. Whereas the adiabatic wave function Ψ^{AD} of Eq. (4) is an exact solution of the three-body equation (with $H_{vc}=-\epsilon_0$) for all $\boldsymbol{R}$ and $\boldsymbol{r}$, the approximation to Ψ^{DW} used in Eq. (10) is introduced as an approximate representation of the elastic distorted wave over only a small region of the configuration space. Clearly this approximate form has nonvanishing overlaps with projectile excitation channels if assumed for all $\boldsymbol{r}$, in contradiction with the definition of Ψ^{DW}. The approximation used in Eq. (10) does not specify an appropriate choice for the direction of the effective momentum $\boldsymbol{K}_a$ which remains a free parameter within that approach. Sensitivity of calculations to its choice are discussed in the following.

In previous work [25,26,35], for s-state projectiles, similar factored expressions for the transition amplitude were obtained by the following steps. First $\boldsymbol{R}$ was replaced by $\boldsymbol{R}_c$ in Eq. (7), termed a ''no-recoil approximation.'' This is seen to be equivalent to assuming $\gamma=0$ in our formulas, requiring $D_0(q)$ to be evaluated at the *large* final state valence particle momentum $q=k_v$. Secondly, despite this requirement, a ZR approximation to the vertex function was made, replacing $D_0(k_v)$ by $D_0(0)$—its small momentum value. These two steps are seen to be inconsistent. The inconsistency arises because, for the heavy projectiles and the beam energies considered here, the distorted waves undergo significant variations over the range of the interaction V_{cv}, and the application of the ZR approximation is unjustified.

In our Coulomb breakup amplitudes the finite-range effects, that $\boldsymbol{R}_c\neq\boldsymbol{R}$, have been retained. The result is that the $D_l(q)$ appear evaluated at momentum q_v or Q_v. In the three-body model used here, momentum transfers to the neutral valence particle can take place only through its interaction with the core particle. The vertex functions describe this momentum transfer from the ground state by V_{cv}. The pres-

ence of the terms involving γ in these transferred momenta is the direct result of treating the finite range effects in the $\boldsymbol{r}$ variable. These momentum transfers take on small values in kinematical regions where the Coulomb breakup amplitudes are large, with the result that relatively low momentum components of the projectile vertices $D_l(q)$ are probed. These are presented in the following section.

D. Expressions for differential cross sections

The triple differential cross section for the elastic breakup reaction is

$$\frac{d^3\sigma}{dE_c d\Omega_c d\Omega_v} = \frac{2\pi}{\hbar v_a}\left\{\frac{1}{2s_a+1}\sum_{\sigma_c\sigma_v\sigma_a}|T_{\sigma_c\sigma_v;\sigma_a}|^2\right\} \times \rho(E_c,\Omega_c,\Omega_v), \tag{15}$$

or, upon carrying out the spin projection summations,

$$\frac{d^3\sigma}{dE_c d\Omega_c d\Omega_v} = \frac{2\pi}{\hbar v_a}\left\{\sum_{l\mu}\frac{1}{(2l+1)}|\beta_{l\mu}|^2\right\}\rho(E_c,\Omega_c,\Omega_v). \tag{16}$$

Here v_a is the a–t relative velocity in the entrance channel. The phase space factor $\rho(E_c,\Omega_c,\Omega_v)$ appropriate to the three-body final state is [36,37]

$$\rho(E_c,\Omega_c,\Omega_v) = \frac{h^{-6}m_t m_c m_v p_c p_v}{m_v+m_t-m_v\boldsymbol{p}_v\cdot(\boldsymbol{P}-\boldsymbol{p}_c)/p_v^2} \tag{17}$$

where, for the differential cross section in the laboratory frame, $\boldsymbol{P}$, $\boldsymbol{p}_c$, and $\boldsymbol{p}_v$ are the total, core, and valence particle momenta in the laboratory system.

The total dissociation cross sections and neutron angular distributions are obtained by integrating the above triple differential cross sections with respect to solid angles and/or energy of the appropriate fragment(s). Starting from the same triple differential cross section, the parallel and transverse momentum distributions of the heavy charged fragment c can be obtained by integration over the unobserved momentum components.

To calculate the c–v relative energy (or excitation) spectrum, we first compute the triple differential cross section $d^3\sigma/dE_{cv}d\Omega_{cv}d\Omega_{(cv)t}$. This is related to the triple differential cross section in Eq. (15) according to [36]

$$\frac{d^3\sigma}{dE_{cv}d\Omega_{cv}d\Omega}_{(cv)t} = \left\{\frac{m_{cv}p_{cv}m_{(cv)t}p_{(cv)t}}{h^6\rho(E_c,\Omega_c,\Omega_v)}\right\}\frac{d^3\sigma}{dE_c d\Omega_c d\Omega_v}. \tag{18}$$

Here the subscripts cv and $(cv)t$ denote relative quantities between the fragments c and v, and the target and center of mass of the two fragments, respectively, and ρ is given by Eq. (17). Integrating over the solid angles Ω_{cv} and $\Omega_{(cv)t}$, one calculates the relative energy spectrum $d\sigma/dE_{cv}$ which, since $E_{ex}=E_{cv}+\epsilon_0$, is equal to the excitation energy spectrum $d\sigma/dE_{ex}$.

III. STRUCTURE MODELS

There is both theoretical [38] and experimental [39] evidence that the ground state of ^{11}Be is, dominantly, a $1s_{1/2}$ neutron configuration. Model calculations suggest a spectroscopic factor $S=0.78$ [38] for this configuration. We calculate the breakup of ^{11}Be assuming a $1s_{1/2}$ neutron orbital with separation energy 0.504 MeV.

For ^{19}C, a simplest shell model picture suggests that the last neutron should be in a $0d_{5/2}$ orbit. More detailed calculations however, based on the Warburton-Brown effective interaction, predict an s-state ^{19}C ground state, due to the lowering of the $1s_{1/2}$ orbit [40]. There is also the possibility, considered in recent model calculations [41], of a $3/2^+$ or $5/2^+$ ground state with a large amplitude of $^{18}\mathrm{C}(2^+;1.62\mathrm{MeV})\otimes s_{1/2}$ configuration. Therefore, for ^{19}C, three sets of calculations will be carried out, with the neutron in either a $1s_{1/2}$ or $0d_{5/2}$ orbit bound by 0.240 MeV, or with the $1s_{1/2}$ neutron bound by 1.86 MeV to a core excited state, which is probably a 2^+ state [42].

We assume a Woods-Saxon potential for V_{cv} with radius and diffuseness parameters 1.15 fm and 0.5 fm, and with depth adjusted to reproduce the bound neutron energies. With this choice the rms radius for the relative motion between the two fragments is 6.7 fm for ^{11}Be. This gives an overall rms radius for ^{11}Be equal to 2.9 fm when the size of the ^{10}Be core is taken as 2.28 fm [43]. For ^{19}C, the valence neutron rms radii are 8.9 fm and 4 fm for the assumed s- and d-states with separation energy 0.240 MeV. The corresponding rms sizes of ^{19}C are 3.45 fm and 2.96 fm. The radius is 3.00 fm for the ^{19}C core-excited s-state configuration. The rms size used for the ^{18}C core is 2.9 fm [44].

Unless otherwise stated we have used these ^{11}Be and ^{19}C wave functions in all calculations. The resulting vertex functions $D_l(q)$ are shown, as a function of q, in Fig. 2.

IV. RESULTS AND DISCUSSIONS

The sensitivity of calculations to the choice of the magnitude and direction of the effective local momentum $\boldsymbol{K}_a$ is of importance in assessing possible quantitative differences in the predictions of the DW and AD approaches.

A. Choice of effective momentum

We first examine the results for a first case, denoted (a), where $\hat{\boldsymbol{K}}_a(R_D)=\hat{\boldsymbol{k}}_a$. We look at the total Coulomb one-neutron removal cross sections σ_{-n} for ^{11}Be on ^{197}Au and ^{19}C on ^{208}Pb at 41 and 77 MeV/nucleon, respectively, as a function of R_D—which controls the magnitude K_a. We find, in all cases considered, that the calculated cross sections increase by order of 10% as R_D increases from 5 to 10 fm, after which there is even less variation (1%). The integrated cross sections are therefore essentially independent of the parameter R_D in the physically plausible region beyond 10 fm. We cannot therefore distinguish between the results of the two models for this choice of $\hat{\boldsymbol{K}}_a$.

The local momentum approximation has been used mostly for nuclear transfer reactions [33,45–48] where there is similar uncertainty regarding the direction to be taken. The authors of Ref. [33] believed that the choice of direction does

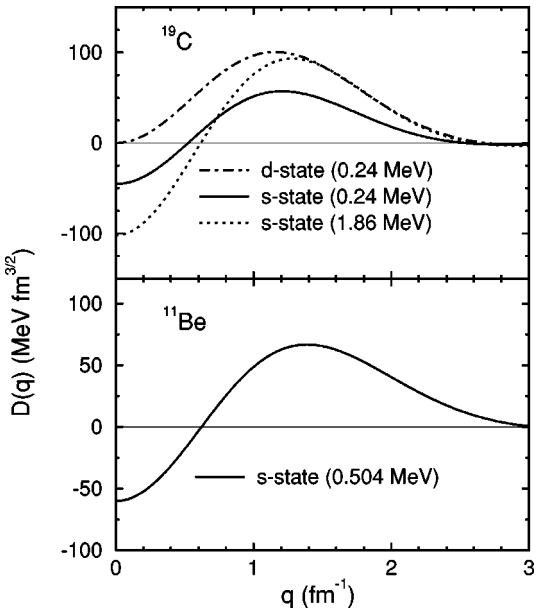

FIG. 2. Vertex functions $D_l(q)$ for ^{19}C and ^{11}Be as a function of momentum transfer q.

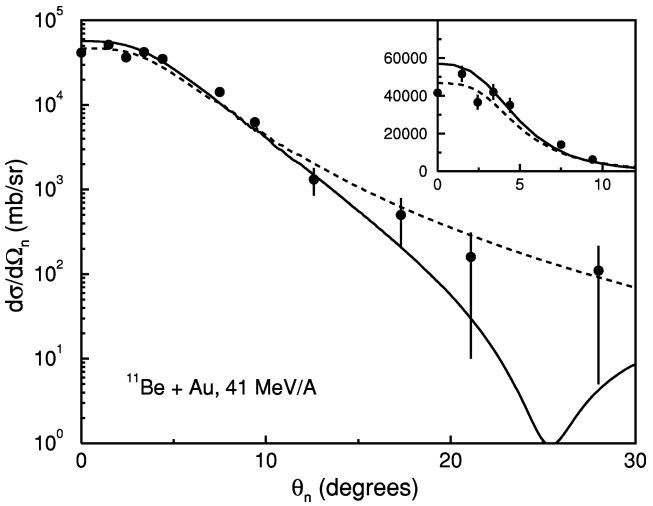

FIG. 3. Exclusive neutron angular distribution for Coulomb breakup of ^{11}Be on Au at 41 MeV/nucleon, with $S=0.78$. The experimental data are from Ref. [11]. The solid line uses case (a) and the dashed line case (c) for the direction of the effective momentum $\boldsymbol{K}_a$.

not affect the results, so they took it along the direction of the corresponding asymptotic momentum. The authors of Ref. [32] assumed that the choice of the direction of $\boldsymbol{K}_a$ does not matter for breakup reactions.

Concerning the validity of a local momentum approximation, in Eq. (11) $\mathcal{R}_{cv}$ is less than 10 fm while the right hand side is greater than 15 fm for all values of R_D used here, when K_a is determined by the Coulomb potential only. Therefore validity can be achieved for pure Coulomb breakup reactions. However, this does not prove the global constancy of $\boldsymbol{K}_a$ over the whole of the configuration space necessary for the calculation of the finite-range DWBA amplitude. This discussion does not arise in the adiabatic formulation.

To study sensitivity to the direction of $\boldsymbol{K}_a$ we have examined two further cases and set $\hat{\boldsymbol{K}}_a$ to the direction of (b) the mean of the incoming and summed outgoing fragment momenta, and (c) the summed outgoing fragment momenta. For ^{11}Be and ^{19}C we see decreases of less than 5% in the cross sections for s-state ground states (see Table I). For a d-state wave function of ^{19}C, (a) and (b) are very similar, but the choice (c) gives very significantly larger cross sections. We also calculate the neutron angular distributions for breakup of ^{11}Be on Au at 41 MeV/nucleon for the case (c), shown by the dashed line in Fig. 3. This angular distribution is broader than the previous one, the peak height somewhat smaller, and there is no minimum at intermediate angles. We observe no dependence of the calculated widths of the parallel momentum distributions of the heavy charged breakup fragment (^{10}Be from Coulomb breakup of ^{11}Be on U at 63 MeV/nucleon) on the direction of $\boldsymbol{K}_a$. The solid curve in Fig. 3 would be changed only at its peak, by of order 3%, if $R_D=10$ fm were used.

We conclude that, in the presented approximation to DWBA, there is some dependence on the choice of the effective momentum $\boldsymbol{K}_a$. This shows up as changes in the cross sections, since $D(\boldsymbol{Q}_v)$ can be very sensitive to small changes in $\boldsymbol{Q}_v$. Within the adiabatic approach, there is no such interpretation or reference to an effective local momentum. The observables that have so far been measured for halo nucleus breakup are not of sufficient precision to distinguish the changes we see here. For the purpose of calculations of the Coulomb breakup of ^{11}Be and ^{19}C, the two approaches give similar results for the observables. We thus concentrate below on what physics can be learned and, unless otherwise stated, we use $\boldsymbol{K}_a=\boldsymbol{k}_a$.

TABLE I. Calculated Coulomb part of σ_{-n} for ^{11}Be and ^{19}C in barns, for the given g.s. spectroscopic factors S and neutron bound state energies ϵ. Columns (a), (b), and (c) correspond to different choices of direction of the effective local momentum of the projectile (see text). The cross sections have been obtained with $R_D>10$ fm (see text).

Projectile + target	ϵ (MeV)	S	E_{beam} (MeV/nucleon)	(a) σ_{-n} s-state	(a) σ_{-n} d-state	(b) σ_{-n} s-state	(b) σ_{-n} d-state	(c) σ_{-n} s-state	(c) σ_{-n} d-state
^{11}Be+^{197}Au	0.504	1	41	2.64		2.64		2.53	
^{11}Be+^{197}Au	0.504	0.78	41	2.06		2.06		1.97	
^{19}C+^{208}Pb	0.240	1	77	3.57	0.37	3.56	0.35	3.49	0.51
^{19}C+^{181}Ta	0.240	1	30	5.30	0.23	5.30	0.23	5.13	0.37
^{19}C+^{181}Ta	1.860	1	30	0.22		0.22		0.20	

TABLE II. Experimental one-neutron removal cross sections σ_{-n} (expt) of ^{11}Be and ^{19}C in barns.

Projectile + target	E_{beam} (MeV/nucleon)	σ_{-n} (expt)	Ref.
^{11}Be+^{197}Au	41	2.5±0.5	[11]
^{19}C+^{208}Pb	77	1.1±0.4	[57]
^{19}C+^{181}Ta	30	0.8±0.3	[53]

B. Total Coulomb one-neutron removal cross sections

Since the majority of the σ_{-n} on targets of high Z is accounted for by Coulomb breakup [25,26], we have made calculations for Pb, Au, and Ta targets. However, as we do not consider nuclear breakup as well as absorption effects, it is not easy for us to calculate realistic total breakup cross sections. For example, we have to perform angular integrations up to 30° for both the fragments in order to obtain convergence of the Coulomb cross sections. Our calculation of the cumulative cross section of ^{11}Be on Au at 41 MeV/nucleon beam energy shows that 10% of the Coulomb breakup is attributable to angles for the total momentum of the projectile fragments beyond 15° and 25% beyond the grazing angle of incidence (8°). Beyond these angles nuclear effects will be predominant but, to compare with published results, we shall present and discuss below the total breakup from the pure-Coulomb dissociation mechanism.

For ^{11}Be on Au at 41 MeV/nucleon we obtain a pure-Coulomb σ_{-n} of 2.06 barns, within the error bounds on the experimental data [see Tables I(a) and II)]. The authors in [11] used a semiclassical theory of Coulomb dissociation, a ZR Yukawa form for the ^{11}Be ground state wave function, together with a finite size correction. They also calculated a cross section of almost 2 barns.

For ^{19}C on Pb at 77 MeV/nucleon and on Ta at 30 MeV/nucleon, our calculated σ_{-n} are 3.6 and 5.3 barns, respectively, when assuming an s-state wave function. These are close to the values of 3.9 and 5.9 barns predicted in a similar core+neutron model by Ridikas *et al.* [41] using semiclassical Coulomb excitation theory with $b_{\min}=10$ fm. The d-state cross sections are an order of magnitude smaller than those for an s-state. This is because q takes on small values (around 0.2 fm^{-1}) at which the vertex function for the d-state is smaller than that for the s-state (Fig. 2). With increase in beam energy, higher values of q contribute to $D(q)$. This explains the increase of the d-state cross sections with beam energy and the corresponding decrease of the s-state cross sections (Table I). Although experimental error bars are large (Table II), comparison with Table I(a) shows that experiment could allow at most 10–17 % of this pure-Coulomb s-state contribution. This is in disagreement with Ref. [4] which concluded that the ground state of ^{19}C is a well-developed s-state neutron halo.

C. Neutron angular distributions

The study of the momentum and angular distributions of fragments emitted in the dissociation of these neutron dripline nuclei is useful in probing the halo structure in their ground state. Distributions of the momenta are related to their spatial distributions by Heisenberg's uncertainty relation. In projectile fragmentation with stable isotopes, under certain conditions the experimental momentum distributions are shown to be proportional to the square of the momentum space wave function of the ground state [27,49]. However, the fragment-target interactions lead to deviations from this simple picture [35,50,51] and, since the Coulomb parts of these interactions are included to all orders in our models, we can investigate the effect of such interactions on the shapes of the fragment momentum distributions.

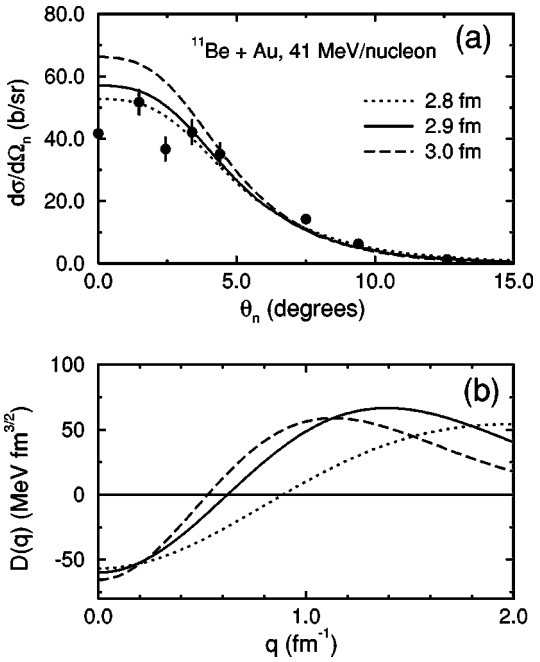

FIG. 4. (a) Neutron angular distributions for ^{11}Be on Au at 41 MeV/nucleon for ^{11}Be wave functions with the rms radii indicated and $S=0.78$. (b) The vertex functions for these wave functions.

In Fig. 3 we show the calculated exclusive neutron angular distribution $d\sigma/d\Omega_n$ (solid line) as a function of θ_n, from the Coulomb breakup of ^{11}Be on a Au target at 41 MeV/nucleon. The experimental data of Ref. [11] are also shown. Exclusive here means that both breakup fragments are detected, but their energies are then summed over. The calculations shown are integrated over the core fragment energy from 390 to 430 MeV, which includes the most significant contributions to the cross section. The angular distribution is forward peaked, reflecting the neutron halo structure [10,11,26,52], and is in good agreement with the experimental data up to angles where nuclear contributions should be considered. There is a minimum in the calculated angular distribution at around 25°, corresponding to the node in the vertex function in Fig. 2, but this is outside the region where the Coulomb mechanism is dominant.

The same distribution, calculated in Ref. [11] using semiclassical theory and a Yukawa wave function, has a dip near 0°. There is also a dip in the experimental data, inset to Fig. 3, but this is not as pronounced as calculated in [11]. We only obtain a dip near 0° if we do not integrate over fragment energies. When we calculate $d^2\sigma/dE_c d\Omega_n$ with the ^{10}Be core moving with exactly the beam velocity, then there is a 3% dip near 0° and a peak at 2°.

The neutron angular distribution also reflects the size of the neutron halo. In Fig. 4 we show neutron angular distributions for ^{11}Be on ^{197}Au at 41 MeV/nucleon for wave func-

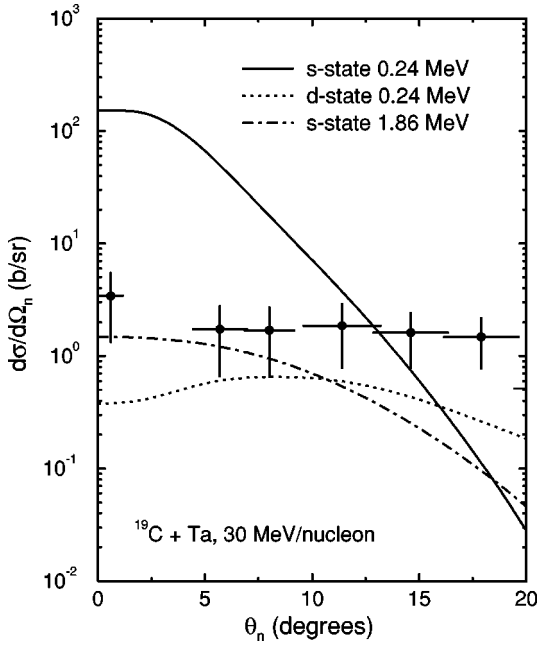

FIG. 5. Neutron angular distributions following Coulomb breakup of ^{19}C on Ta at 30 MeV/nucleon. The solid and dashed lines are for the *s*- and *d*-state configurations with bound state energy 0.24 MeV. The dot-dashed line results from the core-excited *s*-state configuration. The data are from Ref. [53].

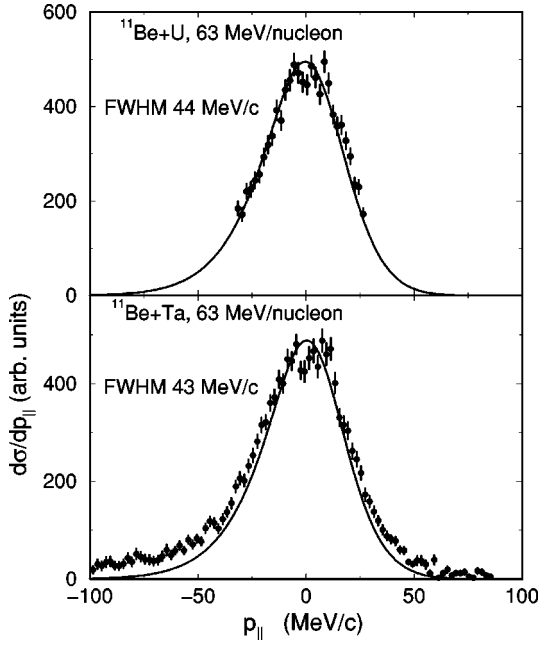

FIG. 6. Calculated parallel momentum distributions of ^{10}Be, following Coulomb breakup of ^{11}Be on U and Ta at 63 MeV/nucleon, in the projectile rest frame. The centroids of the experimental data, from [14], have been shifted to compare the widths.

tions with three different values of the ^{11}Be rms radius. All calculations use $S=0.78$. The solid line is the same as in Fig. 3, with rms radius 2.9 fm. Varying the shape of the Woods-Saxon binding potential to obtain different sizes of the neutron halo, we get the dotted and the dashed lines for ^{11}Be rms radii of 2.8 fm and 3.0 fm, respectively. The different peak magnitudes at forward angles reflect the different values for $D_0(q)$ for $q\approx 0$ (Fig. 4, lower part) from the three wave functions. Improved experimental data could be used to determine the size of ^{11}Be. For a given neutron separation energy, in the analogous zero-range semiclassical or quantum mechanical calculations [11,26] there is only sensitivity to the size of the neutron halo if one renormalizes the ground state wave function from unity, e.g., [9], so as to scale the halo (Yukawa) wave function tail to a realistic amplitude.

The possible amplitude of a *d*-state component in the ground state of ^{19}C could also be observed in the exclusive neutron angular distributions for ^{19}C breakup. These are shown in Fig. 5 for ^{19}C on Ta at 30 MeV/nucleon. The shape and magnitude of the *s*-state angular distribution (upper part) is quite different from that for the *d*-state, whose angular distribution is distinctively broader. This can be understood from the vertex functions shown in Fig. 2. Since increasing scattering angles probe $D_l(q)$ at larger q the cross section increases for the *d*-state and decreases for the *s*-state.

Very recent measurements of ^{19}C one-neutron removal cross sections and neutron angular distributions taken at GANIL [53] therefore give a direct indication of the ground state structure. The magnitude of the cross section at forward angles is expected to have a significant contribution from the Coulomb breakup mechanism calculated here. Recent data in [53], reproduced in Fig. 5, show a broad neutron distribution with a full width at half maximum (FWHM) of 120 ± 18 MeV/c. The cross section magnitude is seen to be $\approx$1.5 b/sr at forward angles. Of our Coulomb breakup calculations, only the model in which the ground state is described as an *s*-wave neutron coupled to a core excited state comes close, both in magnitude and shape, to the data. In this case, we calculate the cross section for detection of the ^{18}C core in the excited (2^+) state. A coherent superposition of $^{18}\mathrm{C}(0^+)\otimes d_{5/2}$ and $^{18}\mathrm{C}(2^+)\otimes s_{1/2}$ configurations is also allowed, for a $5/2^+$ ground state, and would lead to an incoherent superposition of the lower two curves in Fig. 5.

D. Core momentum distributions

In Fig. 6 we show the parallel momentum distributions (PMD) $d\sigma/dp_\|$ as a function of $p_\|$ of the ^{10}Be, for ^{11}Be on U and Ta targets at 63 MeV/nucleon. The calculated and experimental [14] distributions have been shifted in energy and normalized at the peaks so as to compare their widths. The peaks of our calculated PMDs fall at the momenta of the beam velocity and we do not predict post-acceleration of the ^{10}Be fragment in this inclusive observable. The calculated Coulomb breakup distributions are seen to agree quite well with the measured widths for both targets. For the Ta target however, where the data are more extensive, the calculated distribution is seen to underpredict the data for larger $p_\|$, due probably to nuclear breakup contributions at larger angles which we have not included.

Our PMD widths for the U and Ta targets are 44 MeV/c and 43 MeV/c FWHM. Experimentally there is also very little change in these widths with target mass, and also with the probable reaction mechanism. Our widths agree with the value 43.6 ± 1.1 MeV/c [14] averaged from data on Be, Nb, Ta, and U targets. The width of the PMD for ^{11}Be breakup estimated from a simple Serber model calculation [54] is 46 MeV/c which is also close to our calculated values. Since

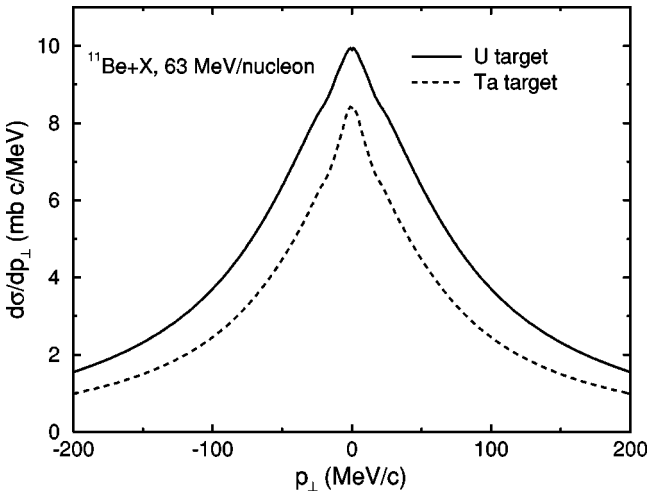

FIG. 7. Transverse momentum distributions of ^{10}Be in the Coulomb breakup of ^{11}Be on U and Ta at 63 MeV/nucleon beam energy.

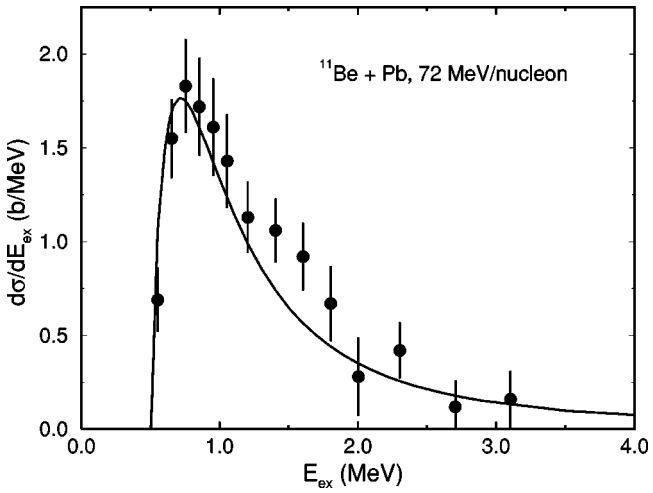

FIG. 8. Excitation energy spectrum for the Coulomb breakup of ^{11}Be on Pb at 72 MeV/nucleon. The data are from [9].

the Serber model does not take into account the effects of the final state fragment-target interactions, and moreover the PMD from this model has no reference to the reaction mechanism, there are strong indications that the PMD provides a measure of the size of the extended s-wave neutron halo for ^{11}Be. More generally, for non-s-wave and/or less extended projectiles, and on light targets, nuclear effects can result in changes in the PMD widths from the intrinsic ones [55,56].

Figure 7 shows the transverse momentum distributions (TMD) $d\sigma/dp_\perp$ as a function of $p_\perp$ of the ^{10}Be, for the same reactions as above. In contrast to the PMD, the transverse widths are broad and are sensitive to the target charge. The FWHM widths change from 110 MeV/c on Ta to 145 MeV/c on U. A similarly broad TMD was observed for ^{9}Li in the reaction of ^{11}Li on Pb [12], which is also Coulomb dominated. This TMD broadening with target charge was not observed in the ZR DWBA calculations of [35]. Since this broadening is sensitive to the fragment-target final state interactions, measured TMD widths do not simply reflect the projectile structure.

E. Excitation energy spectra

The calculated excitation energy spectrum of the ^{10}Be $+n$ system, for ^{11}Be on Pb at 72 MeV/nucleon, is shown in Fig. 8. Also shown are the experimental data of Ref. [9] whose authors estimated the nuclear contributions to be less than 10% at the peak position. They interpreted this as a direct breakup spectrum because they were able to fit the measured excitation spectrum using a dipole strength distribution and a direct breakup model. This use of direct breakup was in the sense of a prior-form DWBA model, rather than the post-form amplitude used here. Their success indicates the low strength of the dipole transition from the ground state. We cannot make a similar claim, since we can derive our post-form results within an adiabatic theory which includes all interactions to higher orders.

Our calculated energy spectrum agrees in shape with that measured, the peak coming around 800 keV. The experimental total dissociation cross section for ^{11}Be is 1.8 ± 0.4 barns [9]. We calculate 1.4 barns (assuming $S=0.78$) from the Coulomb breakup mechanism alone.

V. CONCLUSIONS

We have performed approximate finite-range quantum mechanical calculations of elastic Coulomb breakup of neutron rich nuclei with a single valence neutron. We have formulated practical finite-range calculations using two theoretical approaches which differ considerably in their physical interpretation.

In the adiabatic approach we make the single approximation that the strongly excited core-valence particle relative energies in Coulomb breakup are small. The finite-range breakup amplitude which results is a product of factors describing separately the projectile structure and the dynamics of the reaction, and revealing the sensitivity of breakup reactions to the projectile structure. This factored form can also be obtained by making an effective local momentum approximation in the post form of the DWBA breakup amplitude. Unlike this DWBA formulation, which is first order in the interaction between the core and the valence particles, the adiabatic formulation is nonperturbative. A requirement of both methods is that the Coulomb interaction acts only on a single charged fragment in the two-body composite projectile.

The two theories give rise to different results, dependent on the direction assumed for the effective momentum in the DWBA approach, and which enters that formulation as a free parameter. Unlike semiclassical and quantum mechanical theories which use the zero-range approximation, and which are unable to include possible d-state components of, e.g., ^{19}C, the present work is applicable to projectiles with any relative orbital angular momentum structure between its fragments. We have investigated the one-neutron removal reactions of ^{11}Be and ^{19}C.

For ^{11}Be, both of our theoretical approaches give generally similar results, and the σ_{-n} and neutron angular distributions at forward angles are consistent with experimental data. The neutron angular distributions are sensitive to the size of the neutron halo and so reflect the ground state configuration of the projectile. The neutron halo structure is also

manifest in the very narrow widths of the parallel momentum distributions of the ^{10}Be fragment calculated for Coulomb breakup of ^{11}Be on U and Ta targets, and which are essentially equal. For ^{11}Be, these parallel momentum distributions are rather independent of the interactions governing the breakup process. The transverse momentum distributions on the other hand are much wider and are also affected by Coulomb final state interactions, even for the well developed s-state halo in ^{11}Be. They are unsuitable for probing the halo structure. No post-acceleration effect is calculated in the parallel momentum spectra of ^{10}Be. The shape of the excitation energy spectrum of ^{11}Be, for breakup on a Pb target, and the appearance of a strong peak at a low excitation energy agree with experimental measurements.

For ^{19}C, a comparison of σ_{-n} with available experimental results is consistent with the ^{19}C ground state being a superposition of d- and s-states, but at most 10–17 % of the s-state is allowed by these data. Very recent measurements, taken at GANIL, of the neutron angular distribution from ^{19}C breakup are shown to provide a more direct indication of this ground state structure. A model in which the ground state is described as an s-wave neutron coupled to an excited ^{18}C core gives Coulomb breakup cross sections closest in magnitude and shape to these new data.

ACKNOWLEDGMENTS

The financial support of the United Kingdom Engineering and Physical Sciences Research Council (EPSRC) in the form of Grant No. GR/J95867 is gratefully acknowledged. The authors would like to thank Professor R. C. Johnson for many stimulating discussions and Dr. J. H. Kelley and Dr. T. Nakamura for providing copies of their experimental data. We would like particularly to thank Dr N. A. Orr for making available the new data of Ref. [53], for the neutron angular distribution following ^{19}C breakup, and for his valuable comments on an earlier draft of this work.

[1] See, e.g., *Proceedings of the International Conference on Nucleus-Nucleus Collisions IV*, edited by H. Toki, I. Tanihata, and H. Kamitsubo [Nucl. Phys. **A533** (1992)].
[2] I. Tanihata, Nucl. Phys. **A522**, 275c (1991); T. Kobayashi, *ibid.* **A553**, 465c (1993), and references therein.
[3] P. G. Hansen and B. Jonson, Europhys. Lett. **4**, 409 (1987).
[4] D. Bazin *et al.*, Phys. Rev. Lett. **74**, 3569 (1995).
[5] F. M. Marqués *et al.*, Phys. Lett. B **381**, 407 (1996).
[6] N. A. Orr *et al.*, Phys. Lett. B **258**, 29 (1991), and references therein.
[7] I. Tanihata, T. Kobayashi, O. Yamakawa, S. Shimoura, K. Ekuni, K. Sugimoto, N. Takahashi, T. Shimoda, and H. Sato, Phys. Lett. B **206**, 592 (1988); B. Blank *et al.*, Z. Phys. A **340**, 41 (1991); M. Fukuda *et al.*, Phys. Lett. B **268**, 339 (1991).
[8] D. Sackett *et al.*, Phys. Rev. C **48**, 118 (1993).
[9] T. Nakamura *et al.*, Phys. Lett. B **331**, 296 (1994).
[10] R. Anne *et al.*, Phys. Lett. B **250**, 19 (1990); **304**, 55 (1993).
[11] R. Anne *et al.*, Nucl. Phys. **A575**, 125 (1994).
[12] T. Kobayashi, O. Yamakawa, K. Omata, K. Sugimoto, T. Shimoda, N. Takahashi, and I. Tanihata, Phys. Rev. Lett. **60**, 2599 (1988).
[13] N. A. Orr *et al.*, Phys. Rev. C **51**, 3116 (1995).
[14] J. H. Kelley *et al.*, Phys. Rev. Lett. **74**, 30 (1995).
[15] C. A. Bertulani and G. Baur, Nucl. Phys. **A480**, 615 (1988).
[16] C. A. Bertulani, G. Baur, and M. S. Hussein, Nucl. Phys. **A526**, 751 (1991).
[17] M. S. Hussein, M. P. Pato, and C. A. Bertulani, Phys. Rev. C **44**, 2219 (1991).
[18] G. F. Bertsch and H. Esbensen, Ann. Phys. (N.Y.) **209**, 327 (1991).
[19] H. Esbensen and G. F. Bertsch, Nucl. Phys. **A542**, 310 (1992).
[20] L. F. Canto, R. Donangelo, A. Romanelli, and H. Schulz, Phys. Lett. B **318**, 415 (1993).
[21] C. A. Bertulani, L. F. Canto, and M. S. Hussein, Phys. Lett. B **353**, 413 (1995).
[22] T. Kido, K. Yabana, and Y. Suzuki, Phys. Rev. C **50**, R1276 (1994); **53**, 2296 (1996).
[23] G. F. Bertsch and C. A. Bertulani, Nucl. Phys. **A556**, 136 (1993); C. A. Bertulani and G. F. Bertsch, Phys. Rev. C **49**, 2839 (1994).
[24] H. Esbensen, G. F. Bertsch, and C. A. Bertulani, Nucl. Phys. **A581**, 107 (1995).
[25] R. Shyam, P. Banerjee, and G. Baur, Nucl. Phys. **A540**, 341 (1992).
[26] P. Banerjee and R. Shyam, Nucl. Phys. **A561**, 112 (1993); Phys. Lett. B **318**, 268 (1993); J. Phys. G **22**, L79 (1996).
[27] G. Baur, F. Rösel, D. Trautmann, and R. Shyam, Phys. Rep. **111**, 333 (1984).
[28] G. Baur and D. Trautmann, Nucl. Phys. **A191**, 321 (1972).
[29] G. Baur, R. Shyam, F. Rösel, and D. Trautmann, Phys. Rev. C **28**, 946 (1983).
[30] R. C. Johnson, J. S. Al-Khalili, and J. A. Tostevin, Phys. Rev. Lett. **79**, 2771 (1997).
[31] J. A. Tostevin *et al.*, Phys. Lett. B **424**, 219 (1998); J. A. Tostevin, S. Rugmai, and R. C. Johnson, Phys. Rev. C **57**, 3225 (1998).
[32] R. Shyam and M. A. Nagarajan, Ann. Phys. (N.Y.) **163**, 265 (1985).
[33] P. Braun-Munzinger, H. L. Harney, and S. Wenneis, Nucl. Phys. **A235**, 190 (1974).
[34] A. Nordsieck, Phys. Rev. **93**, 785 (1954).
[35] P. Banerjee and R. Shyam, Phys. Lett. B **349**, 421 (1995).
[36] H. Fuchs, Nucl. Instrum. Methods Phys. Res. **200**, 361 (1982).
[37] G. G. Ohlsen, Nucl. Instrum. Methods **37**, 240 (1965).
[38] F. M. Nunes, I. J. Thompson, and R. C. Johnson, Nucl. Phys. **A596**, 171 (1996).
[39] B. Zwieglinski *et al.*, Nucl. Phys. **A315**, 124 (1979).
[40] E. K. Warburton and B. A. Brown, Phys. Rev. C **46**, 923 (1992).
[41] D. Ridikas, M. H. Smedberg, J. S. Vaagen, and M. V. Zhukov, Europhys. Lett. **37**, 385 (1997); Nucl. Phys. **A628**, 363 (1998).

[42] D. R. Tilley, H. R. Weller, and C. M. Cheves, Nucl. Phys. **A595**, 1 (1995).
[43] J. S. Al-Khalili and J. A. Tostevin, Phys. Rev. Lett. **76**, 3903 (1996).
[44] E. Liatard *et al.*, Europhys. Lett. **13**, 401 (1990).
[45] L. R. Dodd and K. R. Greider, Phys. Rev. **180**, 1187 (1969).
[46] P. S. Hague, Nucl. Phys. **A223**, 394 (1974).
[47] P. Braun-Munzinger and H. L. Harney, Nucl. Phys. **A223**, 381 (1974).
[48] M. A. Nagarajan, Nucl. Phys. **A196**, 34 (1972).
[49] J. Hüfner and M. C. Nemes, Phys. Rev. C **23**, 2538 (1981).
[50] C. A. Bertulani and K. W. McVoy, Phys. Rev. C **46**, 2638 (1992).
[51] P. G. Hansen, in *Proceedings of the International Conference on Exotic Nuclei and Atomic Masses*, Arles, France, 1995, edited by M. de Saint Simon and O. Sorlin (Editions Frontières, Gif-Sur-Yvette, France, 1995), p. 175.
[52] K. Riisager *et al.*, Nucl. Phys. **A540**, 365 (1992).
[53] E. Liegard *et al.*, LPC-Caen report LPCC 98-03 (unpublished); E. Liegard, thèse, Université de Caen, France, 1998.
[54] R. Serber, Phys. Rev. C **72**, 1008 (1947).
[55] P. G. Hansen, Phys. Rev. Lett. **77**, 1016 (1996).
[56] H. Esbensen, Phys. Rev. C **53**, 2007 (1996).
[57] D. Bazin *et al.*, contribution to the Gull Lake Workshop on Nuclear Physics near the Drip-lines, Gull Lake, Michigan, 1996.